Dystrophic skeletal muscle fibers display alterations at the level of calcium microdomains

Marino DiFranco, Christopher E. Woods*, Joana Capote, and Julio L. Vergara†

Department of Physiology, David Geffen School of Medicine, University of California, Los Angeles, CA 90095

Edited by Francisco Bezanilla, University of Chicago, Chicago, IL, and approved July 24, 2008 (received for review March 7, 2008)

The spatiotemporal properties of the Ca^{2+}-release process in skeletal muscle fibers from normal and *mdx* fibers were determined using the confocal-spot detection technique. The Ca^{2+} indicator OGB-5N was used to record action potential-evoked fluorescence signals at consecutive locations separated by 200 nm along multiple sarcomeres of *FDB* fibers loaded with 10- and 30-mM EGTA. Three-dimensional reconstructions of fluorescence transients demonstrated the existence of microdomains of increased fluorescence around the Ca^{2+}-release sites in both mouse strains. The Ca^{2+} microdomains in *mdx* fibers were regularly spaced along the fiber axis, displaying a distribution similar to that seen in normal fibers. Nevertheless, both preparations differed in that in 10-mM EGTA Ca^{2+} microdomains had smaller amplitudes and were wider in *mdx* fibers than in controls. In addition, Ca^{2+}-dependent fluorescence transients recorded at selected locations within the sarcomere of *mdx* muscle fibers were not only smaller, but also slower than their counterparts in normal fibers. Notably, differences in the spatial features of the Ca^{2+} microdomains recorded in *mdx* and normal fibers, but not in the amplitude and kinetics of the Ca^{2+} transients, were eliminated in 30-mM EGTA. Our results consistently demonstrate that Ca^{2+}-release flux calculated from release sites in *mdx* fibers is uniformly impaired with respect to those normal fibers. The Ca^{2+}-release reduction is consistent with that previously measured using global detection techniques.

calcium signals | excitation-contraction coupling | muscular dystrophy | muscle physiology | confocal spot detection

Duchenne muscular dystrophy (DMD), the most common debilitating genetic disorder affecting boys, is caused by mutations that lead to the improper expression of the protein dystrophin, a major component of the dystrophin glycoprotein complex (DGC) in skeletal muscle (1, 2). A great deal of our understanding of the physiological impact of the absence of dystrophin comes from experimental evidence obtained from studies of the *mdx* mouse, an animal model of DMD that exhibits a similar alteration of the DGC (for a review see ref. 3). Nevertheless, the pathophysiology of DMD is far from being understood.

Skeletal muscle fibers from both DMD patients and *mdx* mice display significantly reduced specific force (4–6), whereas the contractile apparatus seems to be normal (7). By recording global Ca^{2+} transients in response to both action potential (AP) stimulation (8) and voltage clamp pulses (9), we have recently demonstrated that the ability of the sarcoplasmic reticulum (SR) to release Ca^{2+} is significantly reduced in *mdx* muscle fibers compared with that of normal mice. Altogether, our results reporting alterations in the physiology of Ca^{2+} release in *mdx* muscle fibers provide a reasonable explanation for muscle weakness in dystrophic fibers.

Our observation that the Ca^{2+}-release flux measured from global detection experiments is reduced in *mdx* muscle fibers, whereas its voltage dependence is unaltered (9), suggests that the impairment likely results from alterations at steps beyond the transduction between the transverse tubule (T-tubule) depolarization and SR Ca^{2+} release. However, it remains to be evaluated whether the overall impairment in Ca^{2+} release observed in global AP- and voltage-clamp-evoked Ca^{2+} transients results from an even impairment of the Ca^{2+} release at every triad, or from the sum of heterogeneous Ca^{2+}-release contributions arising from both normal and impaired triads.

To address this issue experimentally, we used the confocal spot detection technique (10–12) to compare the spatiotemporal properties of AP-evoked Ca^{2+} transients, recorded from several sarcomeres, between normal and *mdx* muscle fibers. We found that the gross spatial distribution of Ca^{2+} microdomains is not altered in *mdx* fibers, but that Ca^{2+}-release flux and other intrinsic properties of the Ca^{2+} microdomains are uniformly altered in this preparation.

Results

OGB-5N Distribution in Normal and *Mdx* Muscle Fibers. We have previously demonstrated that the resting distribution of the Ca^{2+} indicator Oregon-Green488-BAPTA-5N (OGB-5N) in *flexor digitorum brevis* (FDB) muscle fibers from normal mice is not homogeneous but displays a banded pattern in which peak fluorescence maxima colocalize with the Z lines (12). Two-photon laser scanning microscopy (TPLSM) imaging of quiescent *mdx* fibers loaded with OGB-5N and stained with the fluorescent potentiometric indicator 1-(3-sulfonatopropyl)-4-[beta [2-(di-n-octylamino)-6-naphtyl]vinyl] pyridinium betaine (di-8-ANEPPS) [see supporting information (SI) Fig. S1] demonstrates that this is also the case in dystrophic fibers. Intensity profiles obtained from OGB-5N (see Fig. S1*A*) and di-8-ANEPPS images (see Fig. S1*B*), which were acquired simultaneously, show that the OGB-5N fluorescence peaks are precisely centered between two closely spaced consecutive bands of di-8-ANEPPS fluorescence. This verifies that, as shown for normal mammalian fibers (12), the OGB-5N peaks observed in the TPLSM images of *mdx* fibers are in close proximity to the Z lines. Fig. S1*D* demonstrates that these OGB-5N fluorescence maxima are also readily observed in a longitudinal scan of an *mdx* fiber (before stimulation). Fig. S1*D* also illustrates that, as reported in normal fibers with two-photon illumination (12), a few milliseconds after stimulation short lasting fluorescence increases appear at both sides of each of the fluorescence intensity maxima, corresponding to the Z lines.

AP-Evoked Ca^{2+} Microdomains from Normal and *Mdx* Fibers. The concept of Ca^{2+} microdomains, where changes in $[Ca^{2+}]$ are measured as a function of space and time to describe Ca^{2+} source sites (13, 14), has been used to characterize subsarcomeric Ca^{2+} release in frog and mammalian skeletal muscle fibers (11, 12, 15). Ca^{2+} microdomains are constructed by first recording $\Delta F/F$ transients with a low-affinity Ca^{2+} indicator from several successive positions along the axis of the muscle fiber, and then plotting them

Author contributions: M.D., C.E.W., and J.L.V. designed research; M.D., C.E.W., and J.C. performed research; M.D. and J.L.V. analyzed data; and M.D. and J.L.V. wrote the paper.

The authors declare no conflict of interest.

This article is a PNAS Direct Submission.

*Present address: Department of Internal Medicine, S101, Stanford University Hospital and Clinics, Stanford, CA 94305-5109.

†To whom correspondence should be addressed. jvergara@mednet.ucla.edu.

This article contains supporting information online at www.pnas.org/cgi/content/full/0802217105/DCSupplemental.

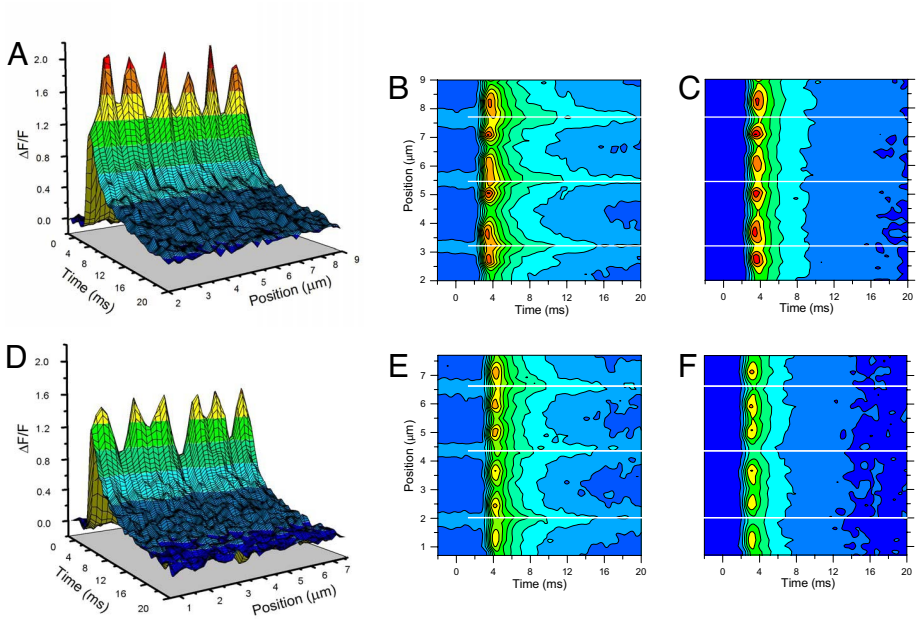

Fig. 1. Calcium microdomains recorded from control and *mdx* fibers. 3-D plots (*A* and *D*) and contour maps (*C* and *F*) of Ca^{2+} microdomains constructed from ΔF/F records acquired from a control (*A* and *C*) and an *mdx* muscle fiber (*D* and *F*). ΔF/F is color-coded with the same palette for 3-D and contour maps. *B* and *E* are fluorescence maps (in arbitrary units and color pallets) corresponding to the ΔF/F maps shown in *C* and *F*, respectively. Solid white lines in *B* and *C* and *E* and *F* indicate the positions of the Z lines.

as a function of the recording position. Fig. 1*A* shows the three-dimensional (3-D) rendition of Ca^{2+} microdomains constructed with data recorded from a normal muscle fiber loaded with 10-mM EGTA. As demonstrated using two-photon illumination (12), this 3-D rendition reveals that the scanned segment of this particular muscle fiber undergoes the formation of six narrow domains of elevated ΔF/F (arranged in three pairs of peaks), which reached their maxima (on average) 4.1 ± 0.04 ms after stimulation, and rapidly dissipated thereafter. Because these domains were obtained using a low-affinity Ca^{2+} indicator in the presence of 10-mM EGTA, we tentatively define them as Ca^{2+}-release microdomains because they may depict the spatiotemporal dependence of $[Ca^{2+}]$ changes (evoked by an AP) in the vicinity of SR Ca^{2+}-release sites (16, 17).

The spatial distribution and time dependence of Ca^{2+} microdomains in Fig. 1*A* can be readily appreciated using contour maps, as shown in Fig. 1*C*. In this representation, reference markers of sarcomere structures can be introduced to indicate the position of the membrane compartments underlying the measured Ca^{2+} release. Accordingly, the positions of the Z lines in the scanned data, determined as explained (see Fig. S1) from a raw fluorescence contour map (Fig. 1*B*), are indicated by solid white lines (see Fig. 1 *B* and *C*). With these references in place, it can be readily observed in Fig. 1*C* that the Ca^{2+} domains flank the Z lines and have their maxima centered at positions coincident with the T-tubule locations (see Fig. S1). Fig. 1*C* also shows that, in a normal fiber, the recorded $[Ca^{2+}]$ changes are minimal at the M lines and intermediate at the Z lines. As illustrated in Fig. 1*C*, the three pairs of Ca^{2+} microdomains (one pair per sarcomere) are distributed at relatively constant intervals with their peaks in the following locations: pair number one, 2.7 and 3.7 μm; pair number two, 5 and 6 μm; and pair number three, 7.1 and 8.2 μm. Obviously, from these positions it was possible to estimate that (for this particular fiber) the distance between pairs of peaks flanking the Z line was ≈1.0 μm ($n = 3$) and the distance across the M line was ≈1.2 μm ($n = 2$). Overall, it is important to note that in a normal fiber, the Ca^{2+} microdomains (see Fig. 1 *A–C*) have similar peak amplitudes (ΔF/F) along its longitudinal axis, are closely synchronized, and are regularly spaced in equivalent sarcomere sites along the distance scanned.

Figs. 1 *D–F* display 3-D and contour map renditions of confocal data obtained from an *mdx* muscle fiber. To facilitate the comparison with data from a normal fiber (see Fig. 1 *A* and *C*), the same scales are used to represent ΔF/F data (see Fig. 1 *D* and *F*). It is obvious from Fig. 1 *D* and *F* that the Ca^{2+} microdomains in *mdx* fibers exhibit similar stereotyped features as those seen in normal fibers: regularly spaced pairs of ΔF/F maxima that are equidistant from the Z line (triads), and smaller ΔF/F changes at the M- and the Z lines. In addition, they display similar amplitude and they are well synchronized. However, it is apparent that both sets of data differ in that the amplitudes of the Ca^{2+} microdomains are uniformly reduced in *mdx* fibers, with respect to those in normal fibers. In addition, unlike what is shown in Fig. 1*C*, the smallest $[Ca^{2+}]$ changes occur at the Z lines in the *mdx* fiber (see Fig. 1*F*).

Confocal Ca^{2+} Transients Recorded at Different Longitudinal Positions in *Mdx* and Control Fibers. As shown (12, 18) and suggested by confocal data from normal fibers described above, AP-evoked localized Ca^{2+} transients display position-dependent amplitudes that are minimal at the center of the sarcomere (midpoint between consecutive Z lines; M-transients), maximal at the triads (T-transients), and intermediate at the Z lines (Z-transients). So far, we have collectively plotted confocal transients to generate 3-D renditions and contour maps of the Ca^{2+} microdomains observed in control and *mdx* fibers (see Fig. 1) to comparatively examine the overall topological features of Ca^{2+} release in each muscle strain. However, careful analysis of the properties of individual confocal Ca^{2+} transients, recorded with high time resolution from selected sites of normal and *mdx* fibers, should allow us to unveil further details about how the positional relationship with respect to underlying anatomical structures may differ in both preparations. Fig. 2*B* shows, superimposed, T-, Z- and M-transients recorded from a control FDB muscle fiber. The corresponding APs for each confocal transient in Fig. 2*B* were identical within ≈2 to 3 mV (Fig. 2*A*); this excludes the possibility that changes in AP amplitude may cause the differences among Ca^{2+} transients recorded at different sarcomere positions. The position-dependent pattern shown in Fig. 2*B* was always observed, even for scan lengths up to 55 μm (i.e., ≈25 sarcomeres). Pooled data, obtained from 10 fibers of nine normal mice, are contained in Table 1. The differences between transient parameters at each location demonstrate that the ΔF/F values of the largest localized transients (T-transients) were significantly larger (≈55%) than the M-transients; in contrast, the difference in amplitude between Z- and M-transients was not found to be significant. As reported while using two-photon illumination (12),

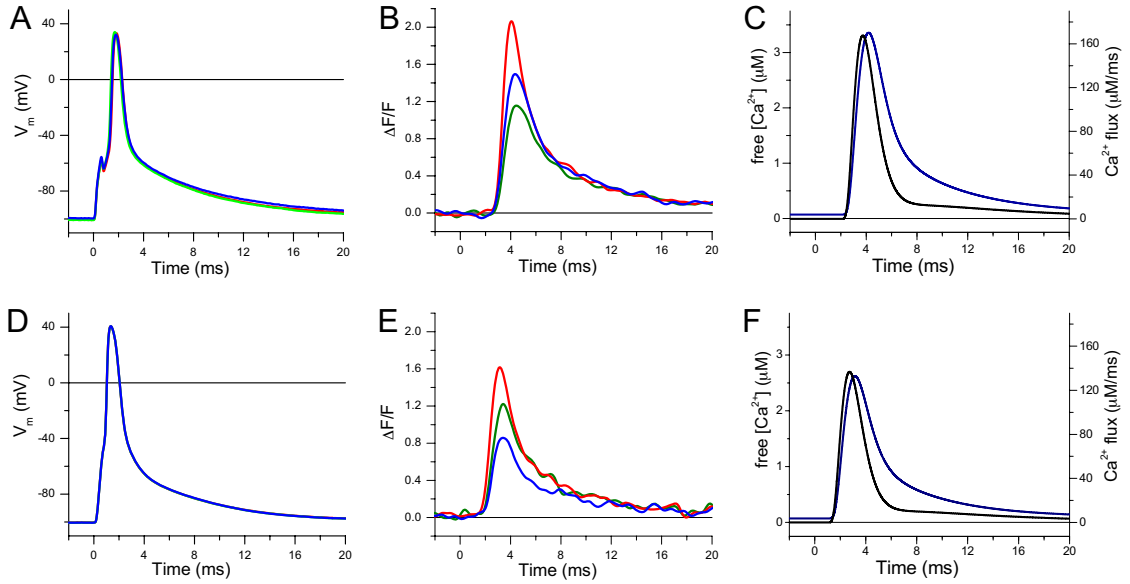

Fig. 2. APs and localized Ca^{2+} transients recorded from control and *mdx* fibers. *A* and *D* are the corresponding AP's that elicited the fluorescence transients in *B* and *E*, respectively. (*B* and *E*) Single-sweep localized ΔF/F transients recorded at the triads (T-positions) (*red traces*), Z lines (*blue traces*) and M lines (*green traces*) of a control (*A*) and an mdx fiber (*D*). (*C* and *F*) Ca^{2+} release flux (*black traces*) and free [Ca^{2+}] changes (*blue traces*) corresponding to the T-transients in panels *B* and *E*, respectively.

the average full-duration-at-half-maximum (FDHM) of M-transients (2.6 ± 0.1 ms; see Table 1) is significantly longer than that of T-transients (2.1 ± 0.1 ms) in normal fibers ($P < 0.05$). Furthermore, the mean amplitude of global transients recorded in association with each scan (data not shown) was found to be smaller, although not significantly, than that of T-transients. The FDHM of global transients was not significantly longer than that of T-transients.

Fig. 2*E* shows localized Ca^{2+} transients recorded from an *mdx* fiber. As seen in control fibers, T-transients were larger than those recorded at the M-position and Z lines. T-transients were also larger than the global transients (data not shown). Furthermore, as in control fibers, the pattern of position-dependent amplitudes of localized Ca^{2+} transients repeats regularly for scans along distances of 20–50 μm (i.e., 8–20 sarcomeres). However, unlike in control fibers, the amplitudes of M-transients were significantly larger (≈14%) than those of Z-transients in *mdx* fibers (see Table 1). In addition, Table 1 shows that, in *mdx* fibers, the average FDHM of M-transients (2.9 ± 0.1 ms) is significantly longer than that of T-transients (2.3 ± 0.03 ms).

In agreement with a previous report (8), we found here that the average amplitude of global Ca^{2+} transients recorded from *mdx* fibers are significantly smaller than those from normal fibers (see Table 1). More importantly, the data in Table 1 shows that localized Ca^{2+} transients recorded at T-, Z- and M-positions from *mdx* fibers are significantly depressed (by at least 21%) with respect to those recorded at corresponding positions in control fibers. Furthermore, the FDHM of localized transients recorded at the T-, Z- and M-positions are longer than those recorded from corresponding positions in control mice (see Table 1). However, it is noteworthy that, although the amplitude of spatially averaged (global) transients is smaller than that of T-transients, no significant difference was found in the duration of global transients recorded from fibers from both strains.

We used a single compartment model of myoplasmic Ca^{2+} buffering (9, 19, 20) to calculate the time course of the Ca^{2+}-release flux and free [Ca^{2+}] change associated with the ΔF/F at the T-positions in Figs. 2 *B* and *D*. In the case of the normal fiber (see Fig. 2*C*) the maximal rate of Ca^{2+} release and the peak free [Ca^{2+}] were 251 μM/ms and 3.4 μM, respectively. The respective values for the *mdx* fiber (see Fig. 2*E*) were 200 μM/ms and 2.6 μM, which represent approximately a 20% and 24% reduction with respect the values in the normal fiber.

In 10-mM EGTA the Ca^{2+} Microdomains Are Wider in *Mdx* than in Normal Fibers. We further characterized the Ca^{2+} microdomains from normal and *mdx* fibers to assess possible differences in the way that Ca^{2+} spreads along the sarcomere in each preparation. This information may prove relevant to understand the impact of Ca^{2+} signaling on the process of contractile activation. Fig. 3*A* (closed

Table 1. Amplitude and duration of localized and global Ca^{2+} transients recorded from normal and *mdx* muscle fibers

	$(\Delta F/F)_{peak}$				FDHM, ms			
	T	Z	M	Global	T	Z	M	Global
Control	2.01 ± 0.03 (200/10)	1.29 ± 0.04 (98/10)	1.33 ± 0.03 (98/10)	1.82 ± 0.10 (11/7)	2.13 ± 0.02 (200/10)	2.62 ± 0.06 (98/10)	2.57 ± 0.06 (98/10)	2.24 ± 0.07 (9/7)
mdx	1.50 ± 0.02 (140/11)	0.92 ± 0.03 (70/11)	1.05 ± 0.02 (73/11)	1.37 ± 0.07 (11/9)	2.33 ± 0.03 (140/11)	3.18 ± 0.13 (70/11)	2.93 ± 0.08 (73/11)	2.35 ± 0.13 (9/9)
Percentage change	−25*	−29*	−21*	−25*	+9.6*	+22*	+14*	+4.9

Values are expressed as mean ± SEM. $(\Delta F/F)_{peak}$ and FDHM are the amplitude and the FDHM of Δ*F*/*F* transients, respectively. T, Z, and M denote confocal transients recorded at specific locations, and "global" denotes transients recorded with global illumination (see text). Percentage change is the decrease (−) or increase (+) of parameter values measured in *mdx* with respect to those measured in control fibers. The asterisk indicates statistically significant changes ($P <$ 0.05). Numbers in parenthesis (*n*/f) are the number of records, *n*, and fibers, f. Data were obtained from seven *mdx* and nine control animals.

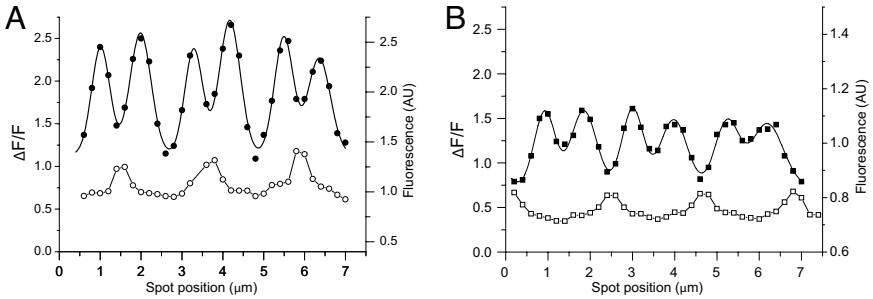

Fig. 3. Width of Ca^{2+} microdomains in control and *mdx* fibers. Filled data points correspond to the ΔF/F value recorded isochronally (2.1 ms after the peak of the AP) at spot positions (separated every 0.2 μm) spanning six Ca^{2+} microdomains. In *A* (*filled circles*) the data were acquired from a control fiber and in *B* (*filled squares*) from an *mdx* fiber. The solid lines through the filled symbols in *A* and *B* are the sum of six Gaussian curves (one per microdomain) fitted to the data. The open symbols represent the prestimulus OGB-5N fluorescence (in arbitrary units) to indicate Z lines' positions.

circles) displays an isochronal ΔF/F profile for a ≈2½ sarcomeres scan, measured at the point when T-transients reached (on average) their maxima, 2.1 ms after the peak of the AP in a control fiber. The average full-width-at-half-maximum (FWHM) of the six microdomains was 0.58 ± 0.05 μm. The open circles in Fig. 3*A*, corresponding to the raw fluorescence of OGB-5N before stimulation, is shown to illustrate the spatial distribution of microdomains with respect to the Z lines. It can be observed that in this normal fiber, the amplitudes of the ΔF/F transients at the Z lines are smaller than those at T-positions, but larger than those at M lines. Fig. 3*B* illustrates the results of a similar experiment for a typical *mdx* fiber. It was found that in this case, the FWHM is 0.67 ± 0.07 μm, which is significantly wider than that of the control fiber. The significance of these differences in FWHM of the microdomains in *mdx*, as compared with control fibers, is sustained in pooled data: the average FWHM, being 0.61 ± 0.015 μm ($n = 52$) and 0.52 ± 0.013 μm ($n = 72$) for microdomains measured from 10 *mdx* and 7 control fibers, respectively. Furthermore, in contrast to what was described for the control fiber, Fig. 3*B* illustrates that at this EGTA concentration, the amplitudes of ΔF/F transients recorded at the Z lines are usually smaller than those of M-transients in *mdx* fibers.

Ca^{2+} Microdomains Recorded in the Presence of 30-mM EGTA. So far we have reported the properties of Ca^{2+} microdomains in *mdx* and normal fibers loaded with 10-mM EGTA. Because this concentration of exogenous Ca^{2+} buffer may not be sufficient to ascertain that free [Ca^{2+}] changes are restrained to the immediate vicinity of the Ca^{2+} sources, as required for our characterization of Ca^{2+}-release microdomains, we used a higher [EGTA] (30 mM). Fig. 4 compares Ca^{2+} microdomains from a normal (see Fig. 4 *A* and *B*) and an *mdx* fiber (see Fig. 4 *C* and *D*) under these conditions. It is observed that the overall stereotyped pattern of Ca^{2+} domains observed at 10-mM EGTA (see Fig. 1) is similarly observed in Fig. 4. Moreover, although the amplitudes of the ΔF/F changes, shown in Fig. 4 for both fiber types, are greatly reduced (because of the higher [EGTA]) with respect to those in Fig. 1, the Ca^{2+} microdomains of the *mdx* fiber are smaller than those in the normal one. The mean amplitude of T-transients from normal and *mdx* fibers were 0.60 ± 0.02 ($n = 15$) and 0.41 ± 0.01 ($n = 17$), respectively. Furthermore, the average FDHM of T-transients recorded in 30-mM EGTA were 1.75 ± 0.02 ms ($n = 15$) and 2.1 ± 0.03 ms ($n = 17$) for normal and *mdx* fibers, respectively. These values are significantly different from each other ($P < 0.05$) even though they are shorter than those shown (both fiber types) in Table 1. Interestingly, the FWHM of the Ca^{2+} microdomains recorded from normal and *mdx* fibers (0.56 ± 0.01 μm and 0.54 ± 0.03 μm, respectively) become indistinguishable in the presence of 30-mM EGTA. Finally, as exemplified in

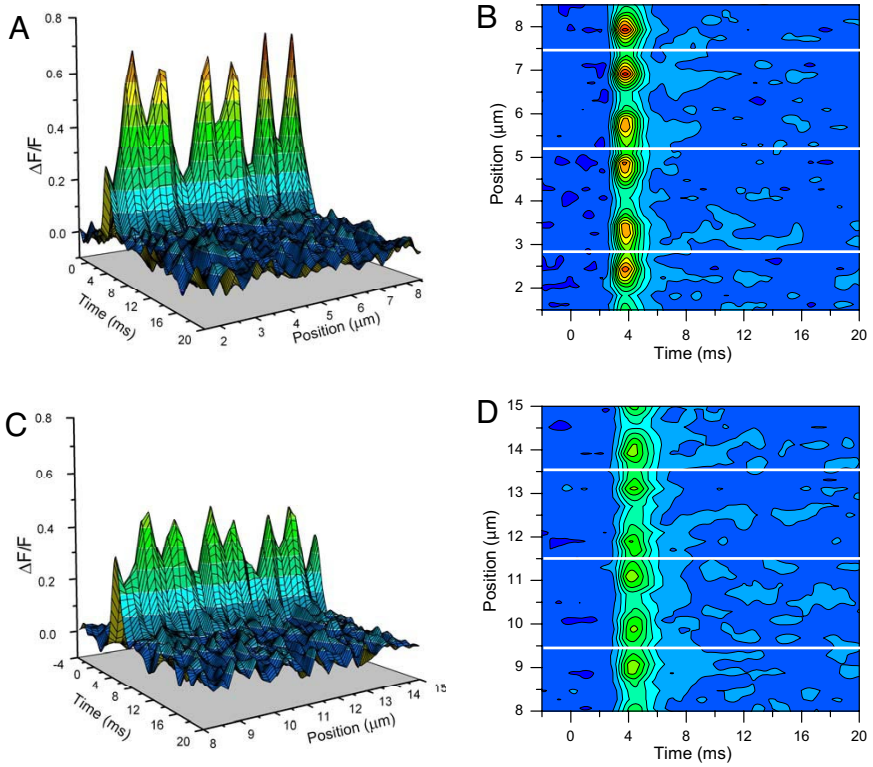

Fig. 4. Calcium microdomains from fibers loaded with 30-mM EGTA. Calcium domains from normal (*A* and *B*) and *mdx* fibers (*C* and *D*) are represented as 3-D plots (*A* and *C*) and contour maps (*B* and *D*), using the same scales and color palettes. The white lines indicate the position of Z lines.

Figs. 4 *B* and *D*, under these conditions the great majority of *mdx* fibers displayed Z line transients larger than the M line transients, thus approximating the pattern found in normal fibers in both 10- and 30-mM EGTA, and in contrast with that found for *mdx* fibers in 10-mM EGTA.

Discussion

In this article, we describe the use of stage-scanning confocal microscopy (spot detection) to record localized AP-induced Ca^{2+} transients within individual sarcomeres of mammalian skeletal muscle fibers isolated from normal and *mdx* mice. Using this approach we obtained a high resolution spatiotemporal portrait of intrasarcomeric Ca^{2+} movements, occurring in response to AP stimulation, which allowed us to refine our knowledge about the functional alterations in the Ca^{2+}-release process that are observed in *mdx* fibers, when compared with normal ones. One of the major discoveries in this realm is that OGB-5N Ca^{2+} transients recorded from *mdx* fibers are homogenously depressed at the level of each microdomain examined. Thus, in 10-mM EGTA, the amplitude of the largest localized transients (T-transients), which correspond to the apex of the microdomains, were (in $\Delta F/F$ units) 1.5 ± 0.02 in dystrophic fibers and 2.01 ± 0.03 for their control counterparts. By using a single compartment kinetic model of the Ca^{2+}-release process (8), which takes into account the concentrations and kinetic properties of most of the relevant myoplasmic Ca^{2+} buffers, including the presence of 10-mM EGTA (8, 9, 20, 21), we calculate the local Ca^{2+}-release flux at T-locations to be 245 ± 5 μM/ms and 185 ± 4 μM/ms for normal and *mdx* fibers, respectively. The values for normal fibers are not dissimilar to those calculated from AP-elicited global transients under comparable experimental conditions (8). Those values for *mdx* fibers (≈24% smaller than normal) are not as depressed as reported for global signals, but still the difference between both strains is significant. The importance of the flux measurements based on localized transients is that the model calculations are validated at the precise location where the Ca^{2+} release is supposed to occur. From these model calculations, we also infer that in 10-mM EGTA the peak free $[Ca^{2+}]$ is 3.3 ± 0.05 and 2.4 ± 0.04 μM at the Ca^{2+}-release sites of normal and *mdx* fibers, respectively. Interestingly, although (as expected) the peak values of local free $[Ca^{2+}]$ at T-positions in the presence of 30-mM EGTA in normal fibers are smaller than those in 10-mM EGTA (1.3 ± 0.03 versus 3.3 ± 0.04 μM), the Ca^{2+} release fluxes predicted by the model at these locations are comparable (234 ± 3 versus 245 ± 5 μM/ms). What is surprising is that in *mdx* fibers the Ca^{2+} release flux calculated from transients in 30-mM EGTA differ substantially from those obtained at 10-mM EGTA (148 ± 5 versus 185 ± 4 μM/ms). Thus, the depression in localized Ca^{2+} release of *mdx* versus normal fibers is much more pronounced at high than at low [EGTA]s (63% versus 24%). We have preliminarily confirmed, in experiments using various [EGTA]s (40-, 30-, 20-, 10-, and 5 mM; semisaturated with Ca^{2+}), that the depression observed in global Ca^{2+} transients from *mdx* fibers is not constant but actually depends on the buffering conditions (22). We believe that this dependence might have important mechanistic implications.

The results reported here disprove the possibility that the reduction in global AP-evoked Ca^{2+} release reported in *mdx* fibers (8), observed in the current experiments, resulted from an underlying alteration in which some of the Ca^{2+} release units remained fully functional, whereas others were significantly impaired. Instead, our Ca^{2+} microdomain data suggest that the Ca^{2+}-release process is uniformly depressed at every triadic location by 24 to 63% (depending on the [EGTA]) in *mdx* with respect to normal fibers. This is an important finding, because it suggests that the absence of dystrophin, a protein putatively restricted to the sarcolemma (23, 24), affects uniformly the voltage-dependent mechanisms of excitation-contraction coupling throughout the fibers' volume. Namely, the stereotyped pattern of Ca^{2+} release, centered at the triads, is maintained in *mdx* fibers, whereas the flux itself is impaired. This finding is consistent with our previous demonstration, confirmed by the data shown in Fig. S1, that the structure of the T-tubular system is preserved in dystrophic fibers from FDB muscles (8). An obvious possible explanation for the persistent depression of Ca^{2+} release in *mdx* fibers is a reduction in the SR Ca^{2+} content. We have recently measured this parameter in fibers from both mice strains by loading them with 6-mM BAPTA and measuring changes in OGB-5N fluorescence upon exposure to 20-mM caffeine (data not shown). The SR Ca^{2+} content, calculated with the same single compartment model used to estimate the Ca^{2+} release flux in AP-evoked transients, was not significantly different in *mdx* fibers with respect to normal controls. This result (M.D. and J.L.V., unpublished work), obtained in fibers from both strains of mice that displayed significant differences in AP-evoked Ca^{2+} release, suggests that the impairment of Ca^{2+} release seen in *mdx* fibers stems from mechanisms other than a reduction in the SR Ca^{2+} content. In view of reports from other laboratories showing that the RyR1 expression in *mdx* muscle fibers seems to be identical to those from normal animals (25), it is likely that functional alterations in the physiological mechanisms that modulate the RyR1 channel opening (or its Ca^{2+} permeability) may be, at least partially, responsible for our observations.

It is interesting that the depression in Ca^{2+} release flux is not the only difference in the spatiotemporal properties of the Ca^{2+} microdomains recorded from normal and *mdx* fibers. We demonstrate in Fig. 3 (and support with pooled data in Table 1) that, under identical experimental conditions, the FDHMs of localized Ca^{2+} transients recorded at selected sarcomeric sites (T-, Z- and M-) of *mdx* fibers are significantly longer than their corresponding ones in control fibers. This reveals a limitation in Ca^{2+} handling by *mdx* fibers that has not been not previously reported, but which may shed light on potential mechanistic deficiencies linked to the SR Ca^{2+} pump (26), parvalbumin (27–29), and calsequestrin (25), previously suggested as potential candidates to explain functional impairments. Curiously, the prolongation in FDHMs demonstrated clearly with the one-to-one comparative analysis of localized transients, is not observed in global transients (see Table 1). Although this finding is in agreement with our previous observations (8), it remains to be elucidated why the averaging involved in the detection of global transients masks the differences in kinetics observed in the local transients recorded from both fiber types.

Another interesting comparative observation that has been made possible by the use of localized detection methods is that, whereas in normal fibers loaded with 10-mM EGTA the $[Ca^{2+}]$ changes observed at the Z lines are similar or larger than those at M line (see Fig. 3), the most common observation in *mdx* fibers is that the transient at the M line is larger than that at the Z line. This is relevant, given the potential role that different regions of the SR (i.e., across the Z line or across the M line), or unevenly distributed endogenous Ca^{2+} buffers, may play on Ca^{2+} signaling and on their alterations in *mdx* fibers. For example, the SR Ca^{2+} pump activity may be lower around the M line in *mdx* fibers as a compensatory response to a smaller Ca^{2+}-release flux at the triads. This could create an asymmetry in Ca^{2+} clearance at both sides of every triad affecting the effective Ca^{2+} binding to troponin. Other factors, such as the accumulation of OGB-5N at the Z lines, probably because of binding to endogenous proteins (11, 30), or the diffusion with binding process of Ca^{2+} toward M- and Z-lines, may be different in normal and *mdx* fibers. Although we cannot readily differentiate among these possibilities, it is interesting that 30-mM EGTA practically eliminates the difference in location for the smallest Ca^{2+} transients (Z line versus M line), which distinguishes normal from *mdx* fibers at lower [EGTA]s. This result suggests that there are spatial differences in endogenous Ca^{2+} buffering (or Ca^{2+} resequestration) between both fiber populations, which were abolished by the use of massive concentrations of the exogenous Ca^{2+} buffer (EGTA). This tentative hypothesis must be tested with more extensive experimentation using other Ca^{2+} buffers (i.e., BAPTA).

It is important to highlight that at least two of the sarcoglycans that participate in the sarcolemmal DGC seem to be localized in the SR as well (31, 32). Their altered expression in *mdx* fibers may impact Ca^{2+} handling in this strain. Whichever the case may be, our experimental observations in 10-mM EGTA demonstrate that *mdx* muscle fibers display significantly wider isochronal Ca^{2+} microdomains than control fibers. This result is difficult to explain because, in principle, 10-mM EGTA in the myoplasm should be sufficient to equalize the spatial distribution of the $[Ca^{2+}]$ in both muscle strains (16, 17). However, the fact that 30-mM [EGTA] was necessary to eliminate FWHM differences between Ca^{2+} microdomains from normal and *mdx* fibers is a practical proof that theoretical calculations underestimated the need of exogenous buffers to dominate sarcomeric heterogeneities endogenous to the muscle fibers.

Materials and Methods

Isolation of Muscle Fibers. Single muscle fibers were enzymatically isolated from FDB and *interosseous* muscles dissected from normal (C57BL/10J) and *mdx* (C57BL/10ScSn-*mdx*/J; Jackson Laboratories) mice as described in ref. 12. Age matched (8–18 weeks old) animals were used. *Mdx* mice at this age are considered to be postnecrotic specimens (33). Animals were handled according to the guidelines laid out by the local University of California Los Angeles Animal Care Committee.

Electrophysiological Techniques, Solutions, and Calcium Measurements. A two-microelectrode amplifier (TEV-200, Dagan) was used to record the membrane potential and to stimulate the fibers, as described (8, 12). Mouse Tyrode and the K-Aspartate internal solution were similar to those described (8, 9). The low affinity *Ca*$^{2+}$ indicator OGB-5N (250 μM) was used to detect myoplasmic $[Ca^{2+}]$ changes. For most experiments, the internal solution contained 10-mM EGTA and 5-mM $CaCl_2$. Some experiments were performed with 30-mM EGTA and 15-mM $CaCl_2$ in the internal solution. These solutions will be referred heretofore as 10- and 30-mM EGTA, respectively. Voltage and current microelectrodes were filled with 1M KCl and internal solution, respectively. Only unbranched *mdx* fibers were used in this study. Experiments were performed at room temperature (20–21°C).

Optical Setup. The optical setup used for global and confocal spot detection was similar to that described to measure Ca^{2+} microdomains in amphibian and mammalian muscle fibers (11, 12). In this case, stage-scanning confocal microscopy used single-photon laser illumination (see below). Localized (confocal spot) and global Ca^{2+} transients could be alternatively detected. For confocal detection, OGB-5N was excited with the 488-nm line of an Argon laser, whereas for global recordings a 100W Tungsten-halogen lamp and a 460 to 500-nm band-pass filter was used (Omega Optical). Identical dichroic mirrors (505DRLP, Chroma Technology) and emission filters (512–558 nm) were used in both configurations. Illumination was controlled with electronic shutters under computer command. A PIN photodiode (HR008, UDT), connected to an integrating patch-clamp amplifier, and a UV-100 diode connected to a nonintegrating patch clamp amplifier, were used to detect OGB-5N fluorescence under confocal and global illumination, respectively. The confocal spot configuration had a spatial resolution of 300 nm in the *xy* plane and 700-nm axial resolution (11).

Fiber Mounting and Confocal Detection of Localized Transients. Fibers were placed on coverslip-bottomed Petri dishes (8), which in turn sat on a custom made *xy* high-resolution scanning-stage driven by two inchworm nanotranslators (EXFO) operating under computer control using a custom-written software (12). Muscle fibers were aligned along either one of the axes of the scanning-stage. The spatial dependence of AP-evoked Ca^{2+} transients was attained by consecutively recording them every 5 s from adjacent sites separated by 200 nm along the long axis of the fiber (12). The scan-length ranged from 10 to 55 μm. Global records were taken before and after the completion of each scan.

Two-Photon Laser Scanning Microscopy. The intracellular distribution of OGB-5N was studied using TPLSM imaging of fibers stained also with di-8-ANEPPS (34). Dyes were excited at 980 nm and their emission was separated with a 450 to 490//550//600 to 640-nm cube. Simultaneous images acquired at both emission bands were superimposed offline to determine the spatial relation between T-tubules and OGB-5N peaks.

Data Acquisition, Analysis, and Statistics. Electrical and optical data (expressed in $\Delta F/F$ units) were filtered at 5 and 2 KHz, respectively, digitalized at 16-bits resolution, and acquired simultaneously. Characteristic parameters of localized and global Ca^{2+} transients were analyzed using custom-written and commercial software as described (11, 12). Free $[Ca^{2+}]$s and Ca^{2+}-release fluxes were estimated from experimental Ca^{2+} transients using a single compartment model (8, 9) and the following (measured) parameters for the OGB-5N dye: $k_{on} = 0.16$ $\mu M^{-1} \cdot ms^{-1}$, $k_{off} = 8\ ms^{-1}$, and $F_{max}/F_{min} = 37$. Two photon images were analyzed using commercial (LaserSharp 2000MP, Zeiss) and public domain image analysis software packages (ImageJ). Results are expressed as mean $\pm$ SEM of n observations. Sets of data were compared using Student's t test with $P < 0.05$.

ACKNOWLEDGMENTS. This work was supported by grants from the Muscular Dystrophy Association of America, and from National Institutes of Health/National Institues of Arthritis and Musculoskeletal and Skin (AR047664 and AR54816), and National Institutes of Health Training Grant GM08042 (to. C.E.W.) (University of California Los Angeles Medical Scientist Training Program).

1. Hoffman EP, Brown RH, Jr, Kunkel LM (1987) Dystrophin: The protein product of the Duchenne muscular dystrophy locus. *Cell* 51:919–928.
2. Emery AE (2002) The muscular dystrophies. *Lancet* 359:687–695.
3. Gillis JM (1999) Understanding dystrophinopathies: An inventory of the structural and functional consequences of the absence of dystrophin in muscles of the mdx mouse. *J Muscle Res Cell Motil* 20:605–625.
4. Watchko JF, O'Day TL, Hoffman EP (2002) Functional characteristics of dystrophic skeletal muscle: Insights from animal models. *J Appl Physiol* 93:407–417.
5. Lynch GS, *et al.* (2001) Force and power output of fast and slow skeletal muscles from mdx mice 6–28 months old. *J Physiol (London)* 535:591–600.
6. Faulkner JA, Brooks SV, Dennis JR, Lynch GS (1997) The functional status of dystrophic muscles and functional recovery by skeletal muscles following myoblast transfer. *Basic Appl Myol* 7:257–264.
7. Williams DA, Head SI, Lynch GS, Stephenson DG (1993) Contractile properties of skinned muscle fibres from young and adult normal and dystrophic (mdx) mice. *J Physiol (Lond)* 460:51–67.
8. Woods CE, Novo D, DiFranco M, Vergara JL (2004) The action potential-evoked sarcoplasmic reticulum calcium release is impaired in mdx mouse muscle fibres. *J Physiol* 557:59–75.
9. Woods CE, *et al.* (2005) Propagation in the transverse tubular system and voltage dependence of calcium release in normal and mdx mouse muscle fibres. *J Physiol* 568:867–880.
10. Escobar AL, Monck JR, Fernandez JM, Vergara JL (1994) Localization of the site of Ca^{2+} release at the level of a single sarcomere in skeletal muscle fibres. *Nature* 367:739–741.
11. DiFranco M, Novo D, Vergara JL (2002) Characterization of the calcium release domains during excitation-contraction coupling in skeletal muscle fibres. *Pflugers Arch* 443:508–519.
12. Gomez J, Neco P, DiFranco M, Vergara JL (2006) Calcium release domains in mammalian skeletal muscle studied with two-photon imaging and spot detection techniques. *J Gen Physiol* 127:623–637.
13. Chad JE, Eckert R (1984) Calcium domains associated with individual channels can account for anomalous voltage relations of CA-dependent responses. *Biophys J* 45:993–999.
14. Neher E (1998) Vesicle pools and Ca^{2+} microdomains: New tools for understanding their roles in neurotransmitter release. *Neuron* 20:389–399.
15. Vergara JL, DiFranco M, Novo D (2001) in *Proceedings of SPIE* (*Biomarkers and Biological Spectral Imaging*), Vol 4259, pp 133–143.
16. Pape PC, Jong DS, Chandler WK (1995) Calcium release and its voltage dependence in frog cut muscle fibers equilibrated with 20 mM EGTA. *J Gen Physiol* 106:259–336.
17. Novo D, DiFranco M, Vergara JL (2003) Comparison between the predictions of diffusion-reaction models and localized Ca^{2+} transients in amphibian skeletal muscle fibers. *Biophys J* 85:1080–1097.
18. Vergara JL, DiFranco M, Novo D (2002) Detection of global and localized Ca^{2+} transients in enzymatically dissociated mouse skeletal muscle fibers. *Biophys J* 82:642a.
19. Woods CE, DiFranco M, Novo D, Vergara JL (2003) Voltage dependence of calcium transients from mammalian skeletal muscle fibers. *Biophysical Society Abstracts* 1161-Pos.
20. Ursu D, Schuhmeier RP, Melzer W (2005) Voltage-controlled Ca^{2+} release and entry flux in isolated adult muscle fibres of the mouse. *J Physiol* 562:347–365.
21. Baylor SM, Hollingworth S (2007) Simulation of Ca^{2+} movements within the sarcomere of fast-twitch mouse fibers stimulated by action potentials. *J Gen Physiol* 130:283–302.
22. Capote J, *et al.* (2008) Alterations in the Dystrophin Glycoprotein Complex (DGC) are Associated with Ca^{2+} Release Impairment in Skeletal Muscle Fibers. *Biophys J* 94:1512.
23. Ervasti JM, Campbell KP (1991) Membrane organization of the dystrophin-glycoprotein complex. *Cell* 66:1121–1131.
24. Durbeej M, Campbell KP (2002) Muscular dystrophies involving the dystrophin-glycoprotein complex: An overview of current mouse models. *Curr Opin Genet Dev* 12:349–361.
25. Culligan K, Banville N, Dowling P, Ohlendieck K (2002) Drastic reduction of calsequestrin-like proteins and impaired calcium binding in dystrophic mdx muscle. *J Appl Physiol* 92:435–445.
26. Kargacin ME, Kargacin GJ (1996) The sarcoplasmic reticulum calcium pump is functionally altered in dystrophic muscle. *Biochim Biophys Acta* 1290:4–8.
27. Klug G, Reichmann H, Pette D (1985) Decreased parvalbumin contents in skeletal muscles of C57BL/6J(dy2J/dy2J) dystrophic mice. *Muscle Nerve* 8:576–579.
28. Sano M, Yokota T, Endo T, Tsukagoshi H (1990) A developmental change in the content of parvalbumin in normal and dystrophic mouse (mdx) muscle. *J Neurol Sci* 97:261–272.
29. Gailly P, Hermans E, Octave JN, Gillis JM (1993) Specific increase of genetic expression of parvalbumin in fast skeletal muscles of mdx mice. *FEBS Lett* 326:272–274.
30. Kurebayashi N, Harkins AB, Baylor SM (1993) Use of fura red as an intracellular calcium indicator in frog skeletal muscle fibers. *Biophys J* 64:1934–1960.
31. Ueda H, Ueda K, Baba T, Ohno S (2001) Delta- and gamma-sarcoglycan localization in the sarcoplasmic reticulum of skeletal muscle. *J Histochem Cytochem* 49:529–538.
32. Estrada FJ, *et al.* (2006) A novel isoform of delta-sarcoglycan is localized at the sarcoplasmic reticulum of mouse skeletal muscle. *Biochem Biophys Res Commun* 340:865–871.
33. Pastoret C, Sebille A (1995) Age-related differences in regeneration of dystrophic (mdx) and normal muscle in the mouse. *Muscle Nerve* 18:1147–1154.
34. DiFranco M, Capote J, Vergara JL (2005) Optical imaging and functional characterization of the transverse tubular system of mammalian muscle fibers using the potentiometric indicator di-8-ANEPPS. *J Membr Biol* 208:141–153.